Geosciences Journal
Vol. 10, No. 4, p. 499 − 505, December 2006

Computational estimation of compaction band permeability in sandstone

Youngseuk Keehm* *Dept. of Geoenvironmental Sciences, Kongju National University, Kongju, 314-701, South Korea*
Kurt Sternlof *Dept. of Earth, Atmospheric, and Planetary Sciences, MIT, Cambridge, MA, USA*
Tapan Mukerji *Dept. of Geophysics, Stanford University, Stanford, CA, USA*

ABSTRACT: Permeability measurements are difficult to obtain when sample availability is restricted, dimensions limited, or materials poorly consolidated. With subsurface cores of sandstone containing thin, tabular compaction bands (CBs), all three challenges can arise. Computational methods for estimating permeability from thin section provide an alternative. We evaluate a new physics-based technique in which lattice-Boltzmann flow simulations are conducted on stochastic realizations of 3D pore structure generated from thin-section images. Applied to the Aztec sandstone of southeastern Nevada, an exhumed analog for CB-rich sandstone aquifers and reservoirs, the estimates agree well with available data—a few millidarcys (CB) to a few Darcys (matrix)—capturing the range of both matrix and CB permeability from a single, representative thin-section. The technique also gives us a tool for estimating permeability anisotropy due to bed types in sandstone. For a subsurface with Aztec equivalent, this result can be invaluable, since pervasive arrays of compaction bands in sandstone have been shown capable of exerting substantial fluid flow effects at scales relevant to aquifer and reservoir management.

Key words: compaction bands, permeability, lattice-Boltzmann method, anisotropy, SEM

1. INTRODUCTION

Compaction bands (CBs) occur in medium to high porosity sandstones as thin, tabular features of porosity-loss compaction accommodated by grain damage, rearrangement and preferential clay accumulation (Fig. 1). Generally from millimeters to a few centimeters in thickness and tens of meters in planar extent, they represent the subset of deformation bands that are dominated by closing-mode displacement and oriented normal to the local direction of maximum compression (Mollema and Antonellini, 1996; Du Bernard et al., 2002; Borja and Aydin, 2004; Sternlof et al., 2005). Reduced porosity, pore connectivity and average pore-throat diameter conspire to decrease deformation band permeability from one to four orders of magnitude relative to the host rock matrix (Pittman, 1981; Freeman 1990; Antonellini and Aydin, 1994; Crawford, 1998; Gibson, 1998; Taylor and Pollard, 2000; Lothe et al., 2002). Sternlof et al. (2004; 2006) have shown that extensive subparallel, subvertical arrays of cm-thick CBs exposed in the upper Aztec sandstone of southeastern Nevada (Fig. 1, map inset) can induce significant reductions in bulk permeability, as well as pronounced permeability anisotropy at scales relevant to production. The Aztec sandstone is a part of a widespread Jurassic eolian system that includes the Navajo and Nugget sandstones (Blakey, 1989). The CBs, which cut across depositional bedding as the oldest structural fabric present, apparently formed in response to compression associated with thin-skinned tectonism of the Cretaceous Sevier Orogeny (Hill, 1989; Eichhubl et al., 2004; Sternlof et al., 2005). The specific hydraulic impacts exerted by CBs in the Aztec depend strongly on their porosity and permeability relative to the surrounding sandstone matrix, as well as on geometrical factors such as average band thickness, spacing, connectivity and volume fraction (Sternlof et al., 2004). While permeability can be relatively easy to evaluate in the matrix, the thinness of CBs renders direct measurement of their permeability difficult and potentially inaccurate under even the best conditions (Antonellini and Aydin, 1994). Given the generally limited availability of material from subsurface aquifers and reservoirs, which may also be weakly consolidated, problems proliferate. Methods for estimating permeability from thin-sections provide an alternative (e.g. Berryman and Blair, 1987; Adler et al., 1990; Blair et al., 1996; Bakke and Øren, 1997). In this paper, we evaluate a new physics-based computational technique with which permeability estimates can be generated from standard, epoxy-impregnated thin sections (Keehm et al., 2004). In order to mimic the real-world conditions of limited sample supply, we apply the method to a single, representative thin section from the Aztec (Fig. 1), and compare the resulting estimations for CB and matrix permeability to actual measurements reported for the Aztec and Navajo sandstones (Antonellini and Aydin, 1994; Flodin et al., 2005).

2. COMPUTATIONAL METHOD

The methodology workflow involves creating a 2D binary image consisting pore space and grains from a digital thin-section image, transforming this into multiple, equally probable stochastic realizations of the full 3D pore structure, and finally applying a lattice-Boltzmann method flow simulation to calculate an effective permeability for each realization (Fig. 2).

*Corresponding author: keehm@kongju.ac.kr

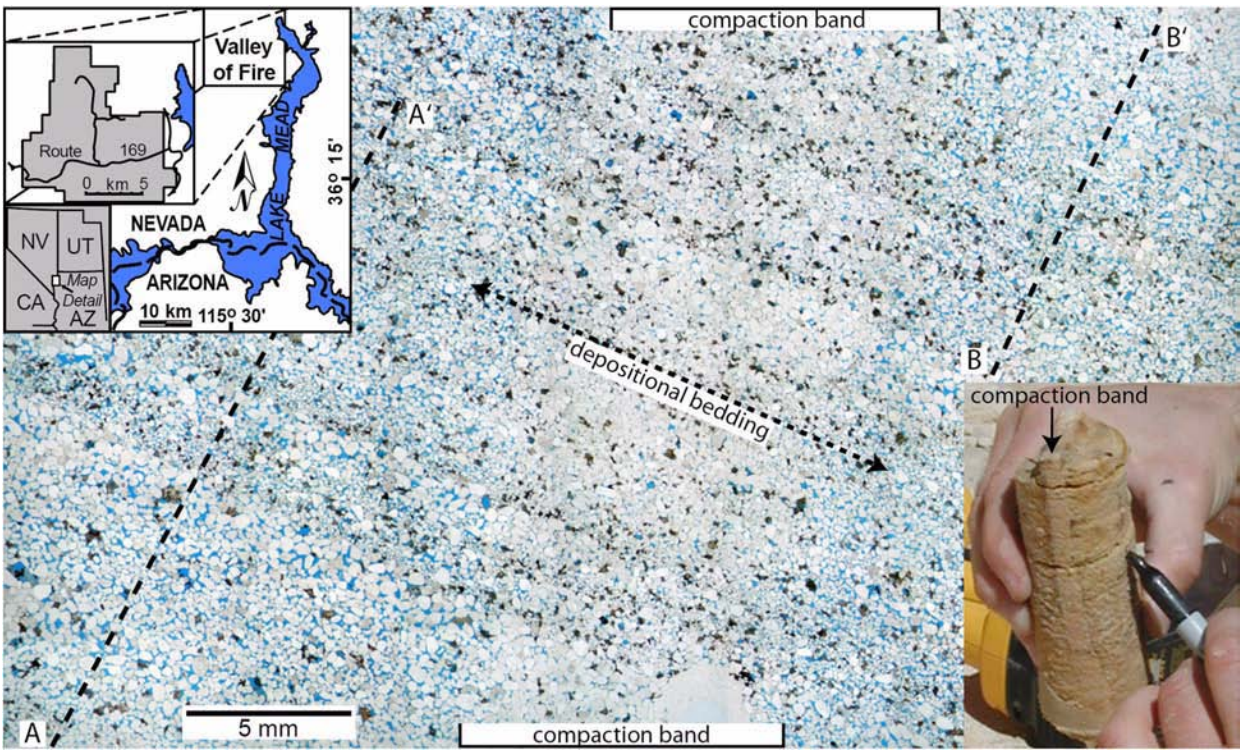

Fig. 1. Representative thin section through a tabular compaction band in the Aztec sandstone. White grains are quartz, brown grains are stained feldspar, black grains are iron oxide, blue is epoxy-filled porosity. Inset map (upper left) shows location of the Valley of Fire in southeastern Nevada. Inset photo (lower right) shows sample core from which the thin section was made. Transects A-A' and B-B' (normal to bedding) pertain to the calculations in Figure 5.

2.1. Image Processing

The first step in estimating permeability from thin-section is to convert representative digital images containing about 100 grains into binary (pure black and white) images (Fig. 2a, b). These binary versions are used for porosity estimation, variogram modeling and as conditional data for the stochastic 3D pore-structure realizations. Two types of initial image are common: true-color RGB (red-green-blue) images captured on standard petrographic microscopes; and grayscale (intensity) images captured with scanning electron microscopy (SEM). With both, the goal is to produce accurate binary maps representing the spatial distribution of pore space and grains. Impregnation with colored epoxy prior to sectioning renders porosity distinct in RGB images. The original method of Keehm et al. (2004) creates a suite of index colors from which an operator selects those corresponding to porosity. With this approach, a degree of uncertainty in the color thresholds differentiating grains from pores is unavoidable. For grayscale images, there is only the intensity plane, with black (low intensity) corresponding to pores. This reduces the binary conversion to a simple choice of threshold value, generally on a scale of 1 (black) to 256 (white). We used SEM images from the representative thin section in this work. To obtain binary images (pore and grain) from SEM intensity images, we chose a threshold and classified each pixel as pore space when the value is less than the threshold, and as grain when otherwise. We chose the threshold of 72 out of 256, after comparing to the measured porosity of the sample. The uncertainty in choosing the right threshold was reasonably small, since unity-offset in threshold gave less than 0.1% of porosity change. Then we can obtain a binary distribution consisting of pore space (black) and grains (white) such as one in Figure 2b. The binary image can be represented by an indicator function, $f(r)$:

$$f(r) = \begin{cases} 1 & \text{if } r \text{ belongs to pore space,} \\ 0 & \text{otherwise} \end{cases} \tag{1}$$

where r denotes spatial location within the binary image. Porosity ϕ and the autocorrelation function $A(\mathbf{h})$, (i.e. the two-point correlation function) can be defined by the statistical averages, denoted by $\langle \cdot \rangle$:

$$\phi = \langle f(r) \rangle, \qquad A(\mathbf{h}) = \langle f(r) f(r+\mathbf{h}) \rangle \tag{2}$$

where $\mathbf{h}$ is a lag vector between two points.

2.2. Realization of 3D Pore Structure

Various methods for constructing 3D pore-structure real-

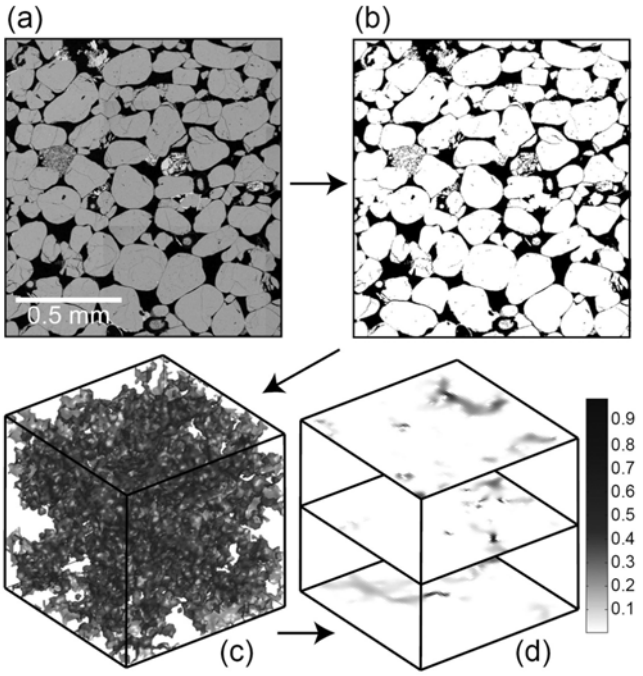

Fig. 2. The workflow of permeability estimation from thin section: (a) compositional backscatter electron image (black=porosity, dark gray=clay, medium gray=quartz, light gray=feldspar); (b) binary image consisting of pore space (black) and grains (white); (c) an example of stochastically simulated 3D pore structures; (d) slices through the pore-structure realization showing local fluid flux predicted by the lattice-Boltzmann flow simulation. Values are normalized by the maximum.

izations from 2D binary images have been developed, including those of Adler et al. (1990), Yeong and Torquato (1998) and Øren and Bakke (2002). A brief comparison of these is presented by Keehm et al. (2004), who offer a geostatistical approach based on the sequential indicator simulation (SIS) method of Deutsch and Journel (1998). The SIS method produces statistical 3D realizations based on the two moments of a binary image—its porosity and the variogram model. The variogram is related to autocorrelation function, except that it reflects the dissimilarity of the data in spatial distribution instead of similarity. The variogram is expressed as follows:

$$\gamma(\mathbf{h}) = \frac{1}{2n(\mathbf{h})}\sum_{i=1}^{n(\mathbf{h})}\{f(r_i) - f(r_i+\mathbf{h})\}^2 = A(0) - A(\mathbf{h}) \qquad (3)$$

where $n(\mathbf{h})$ is the number of pairs of data locations separated by a vector $\mathbf{h}$. This raw experimental variogram contains two-point statistics from the sample; however we need to model the raw variogram using an exponential function to ensure positive-definiteness of the variogram model and to use in the stochastic simulations. The exponential variogram model, which can be obtained by fitting the raw variogram with an exponential function, is as follows:

$$\gamma(\mathbf{h}) = c\ 1\{1 - \exp(-3\mathbf{h}/a)\} \qquad (4)$$

where c is called the sill and a the range of the variogram. With the calculated porosity and the variogram model, we are ready to use SIS to simulate 3D porous media conditioned to the thin section. In the SIS algorithm, a random path is followed through the nodes of a model 3D grid. At each node, a local conditional cumulative distribution function (*ccdf*) for $f(r)$ is estimated by indicator kriging. Each successive *ccdf* is conditioned to the binary image and to all previous node selections, and a random selection from the function gives the value—pore or grain—for the current node. Finally, when all the nodes are visited, a 3D (cubic) binary field with the same pore-grain spatial characteristics as the original image can be obtained (Fig. 2c). Comparing multiple realizations generated from an image provides a statistical measure of pore-structure variability.

2.3. Permeability Estimation

Permeability is estimated by conducting numerical flow simulations on the 3D pore-structure realizations, which generally are geometrically complex and may contain statistical noise due to the stochastic nature of their construction (Keehm et al., 2004). The lattice-Boltzmann (LB) method is a robust technique that simulates flow according to simple rules governing local interactions between individual particles (Doolen, 1990) and recovers the Navier-Stokes equations at the macroscopic scale (Ladd, 1994). Prime advantages of the LB method are its ability to handle any discrete geometry without simplification (Cancelliere et al., 1998), and its accuracy in describing flow through porous media (Ladd, 1994; Bosl et al., 1998; Keehm et al., 2001). Artifacts can occur in the local velocity fields (Manwart et al., 2002), but applying time-averaged velocities mitigates these effects (Ladd, 1994). The LB simulations are accomplished by assigning a pressure gradient (∇P) across opposite faces of the pore-structure cube. From the local fluid flux (Fig. 2d), a volume-averaged flux $\langle q \rangle$ can be calculated. The macroscopic permeability (k) is then calculated according to Darcy's Law:

$$\langle q \rangle = -\frac{k}{\eta}\nabla P \qquad (5)$$

where η is the dynamic viscosity of the fluid. As a statistical measure of k variability, LB simulations can be conducted on multiple 3D pore-structure realizations generated from a given image. The final permeability estimate is then the average of the values from all the simulations.

3. APPLICATION TO THE AZTEC SANDSTONE

In order to test the computational estimation method under real-world conditions of limited supply, we applied

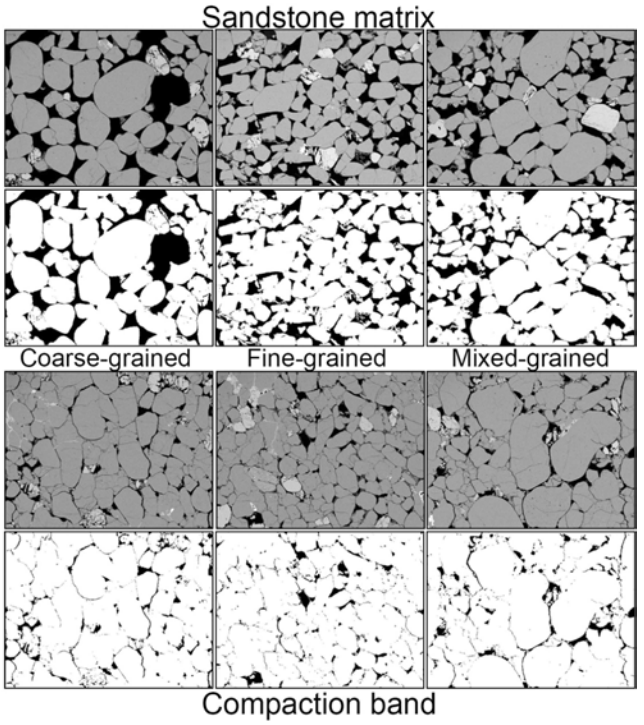

Fig. 3. Compositional backscatter electron images of the three bed types (coarse-grained, fine-grained and mixed-grained) shown above their corresponding binary conversion for both the sandstone matrix and compaction band.

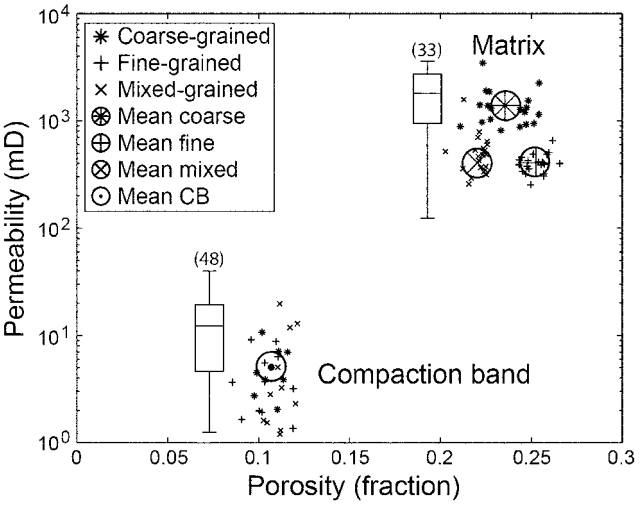

Fig. 4. Semi-log plot of permeability versus porosity for the computational estimates of matrix and compaction band derived from the thin section shown in Fig. 1. Box plots represent the corresponding range and distribution of available permeability measurements from comparable Aztec and Navajo sandstone samples (number of data points in parentheses).

the algorithm to a single, representative thin section of Aztec sandstone showing a cm-thick CB surrounded by relatively undeformed matrix (Fig. 1). As is typical with eolian sandstones, depositional bedding consists of alternating, well-sorted coarse-grained (~0.4 mm) and fine-grained (~0.1 mm) layers up to several millimeters thick. Poorly sorted layers of grain mixing also are common. Within each of the three distinct bed types, the distribution of grains and pores is relatively homogeneous, both in the matrix and in the CB. Compositional backscatter electron images were collected in TIFF format on a standard SEM at 15 kV and 80x magnification. Two images were collected from each bed type, with mosaic composites used as necessary to ensure representative coverage. Thus, we have 12 images (2 images × 3 bed types in the matrix and CB). An intensity threshold of 72 out of 256 was used for the binary conversions, and ten 3D pore-structure realizations were computed for each of the 12 binary images. Figure 3 shows an example image/binary conversion pair for each bed type in both the matrix and the CB. Flow simulations were then conducted on each pore-structure realization to yield 120 total estimates of permeability.

3.1. Simulation Results

The resulting estimates of porosity and permeability are plotted in Figure 4 and summarized in Table 1. Porosity and permeability estimates for the matrix range from about 20-27% and 200-3,500 millidarcys (mD). As expected, mean porosity for the pore-structure realizations derived from the poorly sorted bed images is lowest, while mean permeability estimated for the coarse-grained pore-structure realizations is highest. The combined mean estimates are 23.6% and 776 mD. This simple mean permeability, however, does not account for the layered, inherently anisotropic nature of the sandstone. Figure 5 presents a more realistic approach to estimating bulk directional permeability, which accounts for permeability anisotropy. We show the calculation of bulk permeability parallel and normal to depositional bed-

Table 1. Summary of computational permeability estimates.

	Sandstone Matrix			Compaction Band		
	Coarse	Fine	Mixed	Coarse	Fine	Mixed
Mean	1,392 mD	406 mD	530 mD	5.22 mD	4.29 mD	5.77 mD
Minimum	879 mD	253 mD	258 mD	2.04 mD	1.36 mD	1.20 mD
Maximum	3,459 mD	655 mD	1,574 mD	10.67 mD	9.12 mD	19.73 mD

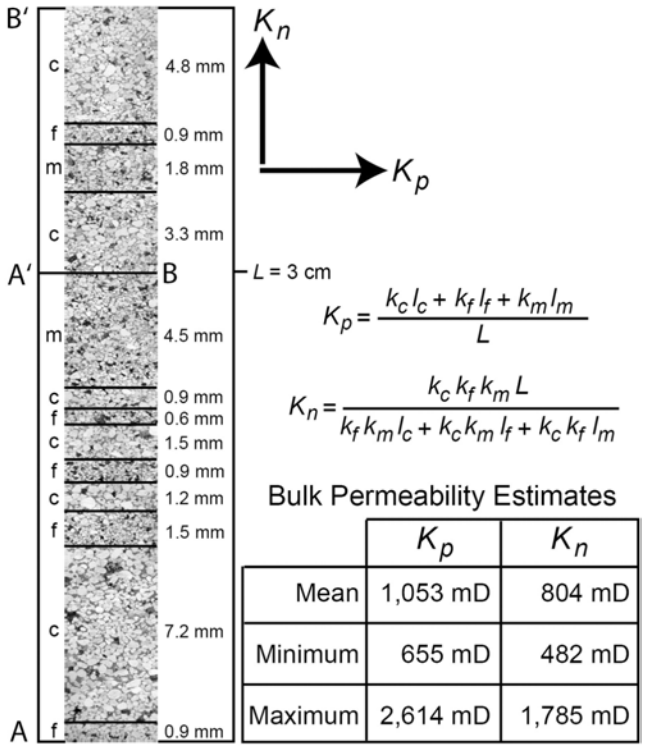

Fig. 5. Calculation of bulk permeability parallel (K_p) and normal (Kn) to depositional bedding for the composite transect A-A'—B-B' shown in Fig. 1. K_p and K_n are calculated as weighted arithmetic and harmonic averages, respectively (Coarse-grained=*c*, fine-grained =*f* and mixed-grained=*m*). Coarse-grained permeability and the total thickness of coarse-grained beds are connoted by k_c and l_c, respectively (k_f, l_f, k_m and l_m follow suit). The mean, min and max bulk permeability estimates were computed using the corresponding values of k_c, k_f and k_m from Table 1.

ding for the composite transect A-A'— B-B' shown in Figure 1. The bulk permeabilities parallel and normal to bedding are calculated as weighted arithmetic and harmonic averages, respectively, using the corresponding values from Table 1. The calculation yields best estimate values of 1,053 mD parallel to bedding and 804 mD normal to bedding. Porosity and permeability estimates for the CB range from about 9-12% and 1-20 mD, with the results from the three bed types substantially overlapping (Fig. 4). This suggests that permeability within the band is approximately homogeneous and isotropic, and the individual estimation for each bed type is not much meaningful. The combined mean estimates for CB porosity and permeability are 10.6% and 5.1 mD. However, exactly half of the 3D pore-structure realizations for the CB—12 for the coarse-grain beds and nine each for the fine-grain and mixed-grain beds—yielded no connected flow paths and so returned zero permeability. Given the minimum non-zero estimate of 1.2 mD, we deemed all zero values to be unrepresentative and discarded them (see Discussion). Our mean estimate of 5.1 mD is therefore a maximum. Including the zero values yields a mean of 2.5 mD, suggesting that the true mean permeability for the CB is probably between 2.5 and 5.1 mD.

3.2. Comparison to Measured Values

Our computational approach yields permeability estimates for the Aztec sandstone of about 1,000 mD along bedding, 800 mD across bedding and 5 mD within CBs, which generally cut across bedding at high angle. Permeability reduction due to compaction within the bands is therefore estimated to be more than two orders of magnitude—the middle of the range reported for deformation bands in general. Antonellini and Aydin (1994) report direct measurements for both matrix and compactive deformation bands from the Navajo Sandstone of southeastern Utah, recognized as a depositional and chronological equivalent of the Aztec (Blakey, 1989). Their results do not distinguish between bedding parallel and bedding normal permeability. Flodin et al. (2005) provide a handful of additional lab measurements for the Aztec matrix. Together, these measurements—ranging from 123 mD to 5,991 mD in the matrix with a mean of 1,768 mD, and from 1.35 mD to 38.33 mD in the bands with a mean of 14.14 mD – correspond quite well with our computational estimates (Fig. 4). In addition, we can obtain the individual permeability estimate for each bed type and the measure of permeability anisotropy.

4. DISCUSSION AND CONCLUSIONS

The method applied in this paper comprises a convenient and robust computational technique for estimating permeability from thin-section images. It is particularly well suited to small structures or samples that do not lend themselves to direct measurement, and to situations where sample supplies are limited or unconsolidated materials requiring impregnation cannot otherwise be analyzed. We have demonstrated that both matrix and compaction band permeability estimates derived from a single thin section of Aztec sandstone reliably reflect the range of measured values reported for comparable samples. Furthermore, we were able to isolate variations in permeability due to grain-size and sorting differences between the characteristic depositional layers—well-sorted coarse, well-sorted fine and poorly sorted mixed—allowing us to assess the inherent permeability anisotropy due to bedding. Application of the method to low-porosity CBs, however, does highlight a resolution issue warranting further comment. The stochastic 3D realization algorithm produces pore structures lacking through-going connectivity with increasing frequency as porosity drops below about 12%. Half of our CB pore-structure realizations, with a mean porosity of 10.6%, yielded zero permeability. Sensitivity testing reveals that below about 7% porosity, the probability of achieving a nonzero permeability result becomes

negligible. The reality for clastic materials is that permeability does not begin to disappear until a minimum porosity threshold of about 2-4% (Mavko and Nur, 1997). This limitation of the method could be mitigated in a variety of ways: e.g. conducting pore-structure realizations until the desired number of non-zero effective permeability results is achieved; increasing resolution of the 3D grid, which would also increases computation time; or using a different 3D pore-structure reconstruction technique such as multipoint realization. We should also comment on the applicability of the method. As mentioned in Keehm et al. (2003), the stochastic methodology we used (SIS) works best on high-porosity clastic rocks such as sandstones, while it has limited successes for carbonate rocks. For crystalline rocks with very low porosity, this method will not be adequate. Nonetheless, we conclude that generally representative permeability estimations can be gleaned from a single, representative thin section using the method demonstrated in this paper. Such data would prove valuable in anticipating and mitigating the bulk impact of CBs on fluid flow in a subsurface equivalent of the Aztec sandstone, with important implications for reservoir and aquifer management and contaminant migration.

ACKNOWLEDGEMENTS: The authors wish to thank David Pollard and Gary Mavko for their insights and support; John Childs for assistance in the field; and Robert Jones for guidance on the SEM. They also thank two anonymous reviewers for the valuable suggestions. Primary funding was provided by the U.S. Department of Energy, Office of Basic Energy Sciences, Geosciences Research Program under grants DE-FG03-94ER14462 and DE-FG02-03ER15423. Additional support came from the Stanford Rock Fracture Project (RFP) and the Stanford Rock Physics and Borehole Geophysics Project (SRB).

REFERENCES

Adler, P.M., Jacquin, C.G. and Quiblier, J.A., 1990, Flow in simulated porous media, International Journal of Multiphase Flow, 16, 691–712.

Antonellini, M., and Aydin, A., 1994, Effect of faulting on fluid flow in porous sandstones: petrophysical properties, AAPG Bulletin, 78, 355–377.

Bakke, S. and Øren, P.E., 1997, 3-D pore-scale modeling of sandstones and flow simulations in the pore networks, SPE Journal, 2, 136–149.

Berryman, J.G. and Blair, S.C., 1987, Kozeny-Carman relations and image processing methods for estimating Darcy's constant, Journal of Applied Physics, 60, 1930–1938.

Blair, S.C., Berge, P.A. and Berryman, J.G., 1996, Using two-point correlation functions to characterize microgeometry and estimate permeabilities of sandstones and porous glass, Journal of Geophysical Research, 101(B9), 20359–20376.

Blakey, R.C., 1989, Triassic and Jurassic geology of the southern Colorado Plateau, in Geologic evolution of Arizona, edited by J.P. Jenny, and S.J. Reynolds, pp. 369-396, Arizona Geological Society Digest, vol. 17.

Borja, R.I., and Aydin, A., 2004, Computational modeling of deformation bands in granular media, I: Geological and mathematical framework, Computer Methods in Applied Mechanics and Engineering, 193, 2667–2698.

Bosl, W.J., Dvorkin, J. and Nur, A. 1998, A numerical study of pore structure and permeability using a Lattice-Boltzmann simulation, Geophysical Research Letters, 25, 1475–1478.

Cancelliere, A., Chang, C., Foti, E., Rothman, D.H. and Succi, A., 1998, The permeability of a random medium: Comparison of simulation with theory, Physics of Fluids A, 2, 2085–2088.

Crawford, B.R., 1998, Experimental fault sealing: shear band permeability dependency on cataclastic fault gouge characteristics, in Structural geology in reservoir characterization, M.P. Coward, M.P. Daltaban, and T.S. Johnson, eds., pp. 27-47, Geological Society of London Special Publications, vol. 127.

Deutsch, C.V., and Journel, A.G., 1998, GSLIB: Geostatistical Software Library and User's Guide, Oxford University Press, New York, 369 p.

Doolen, G.D., 1990, Lattice Gas Methods for Partial Differential Equations, Addison-Wesley, Redwood City, CA, 554 p.

Du Bernard, X., Eichhubl, P. and Aydin, A., 2002, Dilation Bands: A New Form of Localized Failure in Granular Media, Geophysical Research Letters, 29(24), 2176.

Eichhubl, P., Taylor, W.L., Pollard, D.D. and Aydin, A., 2004, Paleofluid flow and deformation in the Aztec sandstone at the Valley of Fire, Nevada--Evidence for the coupling of hydrogeological, diagenetic and tectonic processes, Geological Society of America Bulletin, 116, 1120-1136.

Flodin, E.A., Gerdes, M., Aydin, A. and Wiggins, W.D., 2005, Petrophysical properties and sealing capacity of fault rock from sheared-joint based faults, Aztec sandstone, Nevada, in Fault seals and petroleum traps, edited by Tsuji, Y. and Sorkhabi, R., pp 197-217, AAPG Memoir, vol. 85.

Freeman, D.H., 1990, Permeability effects of deformation bands in porous sandstones, Master's thesis, University of Oklahoma, 90 p.

Gibson, R.G., 1998, Physical character and fluid-flow properties of sandstone-derived fault zones, in Structural geology in reservoir characterization, edited by M.P. Coward, M.P. Daltaban, and T.S. Johnson, pp 83-97, Geological Society of London, Special Publications, vol. 127.

Hill, R.E., 1989, Analysis of deformation bands in the Aztec sandstone, Valley of Fire State Park, Nevada, Master's thesis, University of Nevada, Las Vegas, NV, 68 p.

Keehm, Y., Mukerji, T. and Nur, A., 2001, Computational rock physics at the pore scale: Transport properties and diagenesis in realistic pore geometries, The Leading Edge, 20, 180-183.

Keehm, Y., Mukerji, T. and Nur, A., 2004, Permeability prediction from thin sections: 3D reconstruction and Lattice-Boltzmann flow simulation, Geophysical Research Letters, 31, L04606, doi: 10.1029/2003GL018761.

Ladd, A.J.C., 1994, Numerical simulations of particulate suspensions via a discretized Boltzmann equation, Part 2: Numerical Results, Journal of Fluid Mechanics, 271, 311-339.

Lothe, A.E., Gabrielsen, R.H., Bjornevoll-Hagen, N. and Larsen, B.T., 2002, An experimental study of the texture of deformation bands effects on the porosity and permeability of sandstones, Petroleum Geoscience, 8, 195-207.

Manwart, C., Aaltosalmi, U., Koponen, A., Hilfer, R. and Timonen, J., 2002, Lattice-Boltzmann and finite-difference simulations of permeability for three-dimensional porous media, Physical Review E, 66, 16702-16802.

Mavko, G., and Nur, A., 1997, The effect of percolation threshold in

the Kozeny-Carmen relation, Geophysics, 62, 1480-1482.

Mollema, P.N. and Antonellini, M.A., 1996, Compaction bands: a structural analog for anti-mod I cracks in eolian sandstone, Tectonophysics, 267, 209-228.

Øren, P.E., and Bakke, S., 2002, Process-based reconstruction of sandstones and prediction of transport properties, Transport in Porous Media, 46, 311-343.

Pittman, E.D., 1981, Effect of fault-related granulation on porosity and permeability of quartz sandstone, Simpson Group (Ordovician), Oklahoma, AAPG Bulletin, 65, 2381-2387.

Sternlof, K.R., Chapin, J.R., Pollard, D.D. and Durlofsky, L.J., 2004, Effective permeability in sandstone containing deformation band arrays, AAPG Bulletin, 88, 1315-1329.

Sternlof, K.R., Karimi-Fard, M., Pollard, D.D. and Durlofsky, L.J., 2006, Flow effects of compaction bands in sandstone at scales relevant to aquifer and reservoir management, Water Resources Research, 42, doi:10.1029/2005WR004664.

Sternlof, K.R., Rudnicki, J.W. and Pollard, D.D., 2005, Anticrack-inclusion model for compaction bands in sandstone, Journal of Geophysical Research, 110, B11403, doi: 10.1029/2005JB003764.

Taylor, W.L. and Pollard, D.D., 2000, Estimation of in-situ permeability of deformation bands in porous sandstone, Valley of Fire, Nevada, Water Resources Research, 36, 2595-2606.

Yeong, C.L.Y. and Torquato, S., 1998, Reconstructing random media, II: Three dimensional media from two-dimensional cuts, Physical Review E, 58, 224-238.

Manuscript received November 6, 2006
Manuscript accepted December 21, 2006